Impedance-based Analysis of Interconnected Power Electronics Systems: Impedance Network Modeling and Comparative Studies of Stability Criteria

Chen Zhang, Marta Molinas, *Member, IEEE*, Atle Rygg, Xu Cai

Abstract—**Impedance is an intuitive and effective way for dynamical representation of power electronics devices (e.g. VSCs). One of its strengths towards others is the natural association with circuits. However, impedances of VSCs are locally evaluated via linearization, a process dependent on the angle of the reference frame, thus the reference frame transformation (i.e. rotation) is required before connecting them in circuits for the purpose of network analysis. Although this issue was properly treated in the state-space modeling, a counterpart for the impedance-based analysis, particularly the stability impacts of this rotation have not been thoroughly discussed and worth being clarified. On the other hand, there are fundamental differences in applying the impedance-based stability criteria of a single-VSC system to an interconnected one. Several restrictions as revealed (e.g. sensitivity to partition points of the Nyquist-based analysis), if not properly considered, may lead to inaccurate stability assessments. In this respect, a clarification of three commonly employed impedance-based stability criteria is achieved. At last, the capability of the Nyquist-based analysis in identifying the system's weak point and in facilitating better network design and planning is presented. All the models and analyses are verified by frequency-scanning and time-domain simulations in PSCAD/EMTDC.**

Index Terms—**converter, criterion, impedance, network, stability**

I. INTRODUCTION

NOWADAYS, power electronics devices, e.g. the voltage source converter (VSC), have been widely adopted for the grid-integration of renewable energies [1] as well as the interconnection of asynchronous AC grids by means of high-voltage-dc (HVDC) technologies [2]. In addition to the bulk systems, power electronics devices in micro-grids [3] also exhibit superior capability in improving overall efficiency and flexibility. Due to such a fast growth of power electronics devices in modern electrical systems, new dynamics and stability issues are emerging. The most commonly encountered one would be the small-signal stability, typically occurred in a manner of wide-band oscillations [4] as reported in the wind parks [5] and solar power plants [6].

To study this small-signal stability issue, either the state-space model-based (e.g. [4], [7] and [8]) or the impedance-model-based analysis (e.g. [9]-[14]) can be applied. Recently, the impedance-based method is prevailing since it can be obtained through either analytical modeling or measurement. Also, the interpretation of dynamics could be easier since the concept of impedance is closely and physically related to circuits. There are various techniques to derive the VSC's impedance. In this regard, a thorough review is given in [9], where the *dq* impedance modeling (e.g. [10]-[12]) and the sequence-domain impedance modeling (e.g. [13] and [14]) are most commonly employed. Other impedance modeling methods, e.g. the $\alpha\beta$-based [15], the phasor-based [16], and the *modified* sequence-domain (MSD)-based ([17] and [18]) are also very useful particularly for gaining the insights into the impedance properties, e.g. the mirror-frequency-coupling (MFC) effect [17]. Once the VSC's impedance is derived, small-signal stability issues due to the interaction between the VSC and the grid can be studied (e.g. [19] and [20]) with the (Generalized) Nyquist criterion [21]. A further overview of this respect will be shown in section III.A.

The above-analyses regarding the impedance modeling and stability assessment are extensively discussed for a single-VSC system. When it comes to an interconnected system composed of multiple converters, one could easily associate them (i.e. each converter's impedance) with basic circuit laws to formulate the impedance-network or its equivalents for analysis. For example, [22] and [23] analyzed the sub/super synchronous oscillation of wind farms, whereas in [24] the harmonic resonance issue of wind farms is forcused. However, it should be noted that, since the impedances are locally evaluated via linearization, they are dependent on the angle of the local reference frame where this linearization is performed.

Marta Molinas, Department of Engineering Cybernetics, Norwegian University of Science and Technology, Trondheim, Norway (marta.molinas@ntnu.no).

Atle Rygg, Department of Engineering Cybernetics, Norwegian University of Science and Technology, Trondheim, Norway (email: atle.rygg@ntnu.no).

Xu Cai, Department of Electrical Engineering, Shanghai Jiao Tong University, Shanghai, China (email: xucai@sjtu.edu.cn).

Therefore, a rotation (i.e. reference-frame transformation) is required before connecting them in circuits. Although this issue was properly treated in the state-space modeling (e.g. [8]), a counterpart for impedance-based analysis, particularly the stability impacts of this rotation have not been thoroughly discussed and worth being clarified.

On the other hand, once the rotation issue for accurately formulating the impedance network is addressed, impedance-based stability criteria (e.g. the Nyquist criterion [20], the loop impedance-based criterion [22], etc.) can be applied for stability assessments. However, there are fundamental differences in applying the impedance-based stability criteria of a single-VSC system to the interconnected one. The restrictions of which, as will be revealed and clarified in this work, if not properly addressed, may lead to inaccurate stability assessments as well.

Therefore, this work aims to address those two concerns, thus is naturally composed of two parts: 1) the first part is section II, which is dedicated to the accurate formulation of the impedance network. In which, the properties and impacts of the rotation on aggregated impedances and stability are discussed and clarified. 2) The second part is composed of section III and section IV, which are dedicated to the stability analysis of the impedance network. First, in section III, three types of commonly employed stability criteria are compared regarding their restrictions and conditions. Then, section IV opens the discussion on the identification of the system's weak point, which is one of the main objectives of stability assessments and is crucial for network design and planning when new components are going to be connected to the existing networks.

II. Accurate Impedance Network Modeling and Impacts of Rotation on Impedance Characteristics

A. Brief introduction of the VSC impedance model

Fig. 1 shows a typical grid-tied VSC system with an inner current-control-loop (CCL), a phase-locked loop (PLL), and an outer control loop. The CCL and PLL are fundamental controls for a grid-synchronized VSC, whereas the outer loop can be freely designed as e.g. the dc voltage or power control.

Recently, extensive works are dedicated to the PLL dynamics, particularly under a weak ac grid. Its effects on either small-signal [25] or large-signal [26] stability are discussed in depth. One of the PLL effects on impedance is the occurrence of dq-asymmetry [27], e.g. for a typical dq impedance [12]:

$$\begin{bmatrix} U_d(s) \\ U_q(s) \end{bmatrix} = \begin{bmatrix} Z_{dd}(s) & Z_{dq}(s) \\ Z_{qd}(s) & Z_{qq}(s) \end{bmatrix} \begin{bmatrix} I_d(s) \\ I_q(s) \end{bmatrix} = \mathbf{Z}_{dq}(s) \begin{bmatrix} I_d(s) \\ I_q(s) \end{bmatrix} \quad (1)$$

the dq symmetry [27] or the Y-symmetry (as proposed in an early work [28]) is stated as the condition $Z_{dd}(s) = Z_{qq}(s)$, and $Z_{dq}(s) = -Z_{qd}(s)$, otherwise, it is dq asymmetric.

Intuitively, most of the linear passive elements are dq symmetric systems, whereas the VSCs are not due to the unequal impacts of VSC controls (e.g. the PLL/dc voltage/active and reactive power) on the d- and the q-axis. Also, the properties of the dq asymmetry could be better illustrated if the MSD impedance [17] is used. In fact, the MSD-
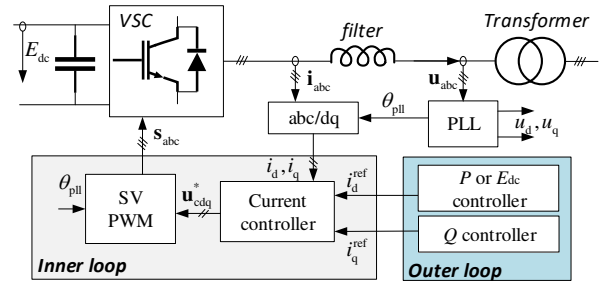

Fig. 1 Schematic of a typical grid-tied VSC system

impedance can be transformed from the dq impedance by applying the concept of symmetrical decomposition [29] as

$$\mathbf{Z}_{pn}(s) = \mathbf{T}_{sym} \cdot \mathbf{Z}_{dq}(s) \mathbf{T}_{sym}^{-1} = \begin{bmatrix} Z_{pp}(s) & Z_{pn}(s) \\ Z_{np}(s) & Z_{nn}(s) \end{bmatrix} \quad (2)$$

where the linear transformation is $\mathbf{T}_{sym} = \frac{1}{2}\begin{bmatrix} 1 & j \\ 1 & -j \end{bmatrix}$. The notation "pn" of lower-case denotes the *modified* sequence-domain different from the *original* one [13].

Besides, it is seen that one of the merits using the MSD impedance is the intrinsic associations with the dq symmetry or diagonality of the matrix. One may easily verify that $Z_{pn}(s) = Z_{np}(s) = 0$ if it is dq symmetric.

B. Properties and impacts of the impedance rotation on the AC coupled systems

A simplified but representative AC coupled system is shown in Fig. 2 (a), where all the VSCs are PQ controlled (see appendix for the models). Since the impedances of the VSCs are locally developed, they only characterize the local behavior of currents and voltages (e.g.$\Delta \mathbf{u}_{dq1}, \Delta \mathbf{u}_{dq2}$ in Fig. 2 (b)). To allow the circuit operations, variables should be in a unified domain, which means they should be transformed into a global/common reference frame. In this study, the global frame
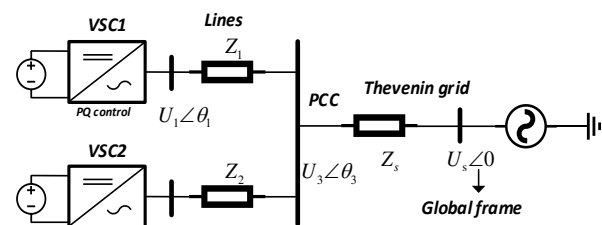
(a) Schematic of an AC coupled system
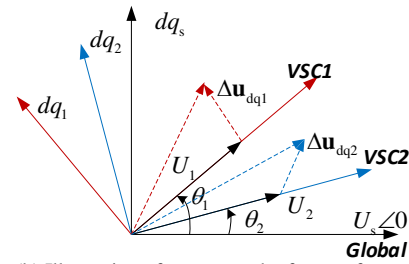
(b) Illustration of vectors and reference frames

Fig. 2 A simple interconnected AC power electronics system

is chosen as the infinite bus-bar, i.e. the dq_s frame in Fig. 2 (b). In fact, the global frame can be arbitrarily chosen as will be

further discussed in section II.C. Based on this definition, variables of dq_1 e.g. Δu_{dq1} can be related to the ones of dq_s through this equation:

$$t\text{-domain}: \begin{bmatrix} \Delta u_{d\_dq1} \\ \Delta u_{q\_dq1} \end{bmatrix} = \begin{bmatrix} \cos\theta_1 & \sin\theta_1 \\ -\sin\theta_1 & \cos\theta_1 \end{bmatrix} \begin{bmatrix} \Delta u_{d\_dqs} \\ \Delta u_{q\_dqs} \end{bmatrix} \quad (3)$$

where θ_1 is the angle difference between dq_1 and dq_s (can be obtained from the load flow analysis). Due to the time-invariance of this transformation, it is valid for s-domain analysis, hence the following equations are obtained:

$$s\text{-domain}: \begin{bmatrix} U_d^{dq1}(s) \\ U_q^{dq1}(s) \end{bmatrix} = \underbrace{\begin{bmatrix} \cos\theta_1 & \sin\theta_1 \\ -\sin\theta_1 & \cos\theta_1 \end{bmatrix}}_{\mathbf{T}_{dq}(\theta_1)} \begin{bmatrix} U_d^{dqs}(s) \\ U_q^{dqs}(s) \end{bmatrix}$$

$$MSD: \begin{bmatrix} U_p^{dq1}(s+j\omega_1) \\ U_n^{dq1}(s-j\omega_1) \end{bmatrix} = \underbrace{\begin{bmatrix} e^{-j\theta_1} & 0 \\ 0 & e^{j\theta_1} \end{bmatrix}}_{\mathbf{T}_{rot}(\theta_1)} \begin{bmatrix} U_p^{dqs}(s+j\omega_1) \\ U_n^{dqs}(s-j\omega_1) \end{bmatrix} \quad (4)$$

where $\mathbf{T}_{rot}(\theta_1)$ is the rotation matrix in the MSD. Applying $\mathbf{T}_{dq}(\theta_1)$ and $\mathbf{T}_{rot}(\theta_1)$ to (1) and (2), the rotated impedances

$$MSD: \mathbf{Z}_{pn}^{global}(s) = \mathbf{T}_{rot}(-\theta_1)\mathbf{Z}_{pn}^{local}(s)\mathbf{T}_{rot}(\theta_1)$$

$$dq: \mathbf{Z}_{dq}^{global}(s) = \mathbf{T}_{dq}(-\theta_1)\mathbf{Z}_{dq}^{local}(s)\mathbf{T}_{dq}(\theta_1) \quad (5)$$

in the global frame are found, where $\mathbf{Z}_{pn}^{local}(s)$ and $\mathbf{Z}_{dq}^{local}(s)$ are the local ones. Based on this, some relevant properties of the rotation in view of MSD-impedances are revealed:

P.1 The MSD-impedance is invariant in terms of the rotation if it is dq-symmetric;

P.2 If it is not dq-symmetric, the rotation only affects the off-diagonal phase of a single MSD-impedance;

P.3 Eigen-loci of a single MSD-impedance is not affected by the rotation, this may *not* be true for aggregated impedances.

These properties are easily proven by expanding (5), i.e.

$$\mathbf{Z}_{pn}^{global}(s) = \begin{bmatrix} Z_{pp}^{local}(s) & Z_{pn}^{local}(s)e^{j2\theta_1} \\ Z_{np}^{local}(s)e^{-j2\theta_1} & Z_{nn}^{local}(s) \end{bmatrix} \quad (6)$$

from which P.1 and P.2 are verified directly. P.3 is justified by further calculating $\det(\lambda\mathbf{I} - \mathbf{Z}_{pn}^{global}) = 0$, where

$$\det\left(\lambda\mathbf{I} - \mathbf{T}_{rot}(-\theta_1)\mathbf{Z}_{pn}^{local}(s)\mathbf{T}_{rot}(\theta_1)\right) = 0$$

$$\rightarrow \det\left(\lambda\mathbf{I} - \mathbf{Z}_{pn}^{local}\right) = 0 \quad (7)$$

Next, the rotation effects on an aggregated impedance will be analyzed, for which the impedances seen from the point-of-common-coupling (PCC, in Fig. 2 (a)) with and without the rotation are first calculated, they are

$$\mathbf{Z}_{pn\_pcc}^{global} = \left(\mathbf{Z}_1 + \mathbf{Z}_{pn\_vsc1}^{global}\right) \| \left(\mathbf{Z}_2 + \mathbf{Z}_{pn\_vsc2}^{global}\right)$$

$$\mathbf{Z}_{pn\_pcc}^{local} = \left(\mathbf{Z}_1 + \mathbf{Z}_{pn\_vsc1}^{local}\right) \| \left(\mathbf{Z}_2 + \mathbf{Z}_{pn\_vsc2}^{local}\right) \quad (8)$$

where $\mathbf{Z}_{pn\_vsc1,2}^{global} = \mathbf{T}_{rot}(-\theta_{1,2})\mathbf{Z}_{pn\_vsc1,2}^{local}\mathbf{T}_{rot}(\theta_{1,2})$. Line impedances ($\mathbf{Z}_{1,2}$) are invariant of rotation according to P.1. Clearly, $\mathbf{Z}_{pn\_pcc}^{global} \neq \mathbf{Z}_{pn\_pcc}^{local}$ if $\theta_{1,2} \neq 0$. And, if the load angles of VSC1 and VSC2 are different, i.e. $\theta_1 \neq \theta_2$, the rotation will affect all the entries of the aggregated impedance matrix.

In order to see the effects clearly, impedance plots of $\mathbf{Z}_{pn\_pcc}^{global}$, $\mathbf{Z}_{pn\_pcc}^{local}$ in comparison with the simulation frequency-

scanning results are shown in Fig. 3. Overall, the impedances with the rotation are consistent with the frequency-scanning results, whereas the ones without the rotation exhibit some errors, justifying the necessity of the rotation and the accuracy of the analytical models.

In detail, since the VSC1 and VSC2 are loaded differently in this case (i.e. $\theta_1 \neq \theta_2$), it is seen that the rotation affects all the entries of the aggregated impedances as expected. By comparing Case I and Case II, one may further observe that the rotation effect of Case I is less evident than that of the Case II. This is due to the small load angles resulting from the small line impedances for Case I. If $\theta_1 \neq \theta_2$ and they are large in magnitudes, the rotation impacts on all the four entries will be evident as illustrated in Case II. This also implies a fact that the eigen-loci of the local and global aggregated impedance will be different, thus leading to different stability conclusions.

However, there exists a special case that the rotation may not
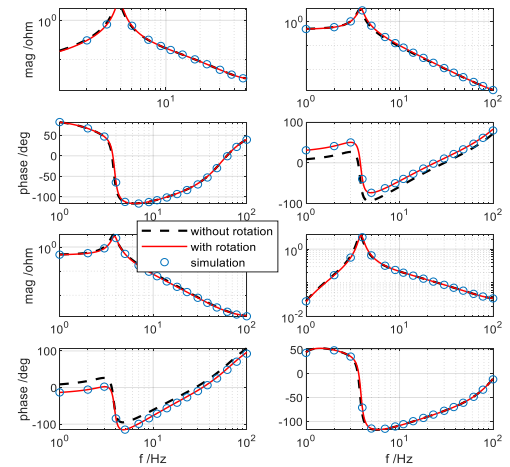
(a) Case I: under a small line impedance ($Z_1 = Z_2 = 0.05$ j p.u)
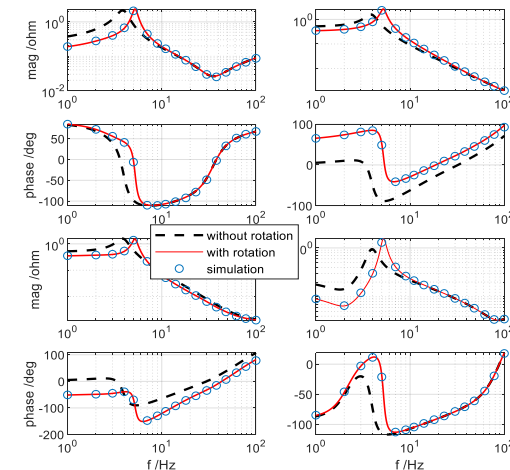
(b) Case II: under a large line impedance ($Z_1 = Z_2 = 0.2$ j p.u)

Fig. 3 The rotation effect on the aggregated impedance of the AC coupled system ($P_{vsc1} = 1.0$ p.u.; $P_{vsc2} = -0.5$ p.u.; $Z_s = 0.125$ j p.u; PLL = 20 Hz, CC = 400 Hz, PQ = 20 Hz; frequency-scanning is from 1 to 100 Hz with 20 points in logarithmic space)

affect the stability conclusion. For instance, if VSC1 and VSC2 are loaded identically i.e. $\theta_1 = \theta_2$, the rotation will merely affect the off-diagonal phases of the aggregated impedances, see Fig. 4 (a), where the off-diagonal phases are oppositely

This article has been accepted for publication in a future issue of this journal, but has not been fully edited. Content may change prior to final publication. Citation information: DOI 10.1109/JESTPE.2019.2914560, IEEE Journal of Emerging and Selected Topics in Power Electronics

> REPLACE THIS LINE WITH YOUR PAPER IDENTIFICATION NUMBER (DOUBLE-CLICK HERE TO EDIT) <　　　4

shifted by an identical magnitude (this is also easily checked by imposing the condition $\theta_1 = \theta_2$ on (8)). Under such a condition, the eigen-loci (with and without rotation) will be identical according to P.3, as a result of which stability conclusions with and without rotation will be identical as well, this is further justified by the Nyquist plots in Fig. 4 (b).
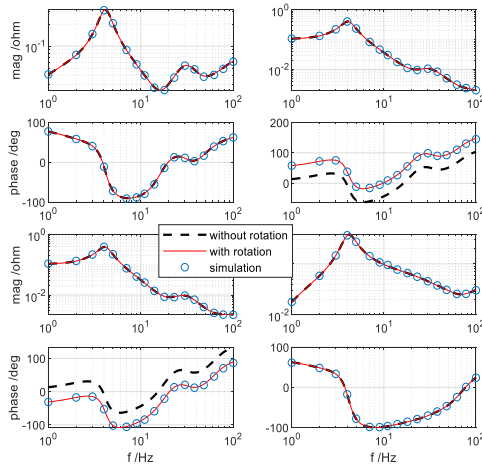
(a) Comparison of the impedance plots
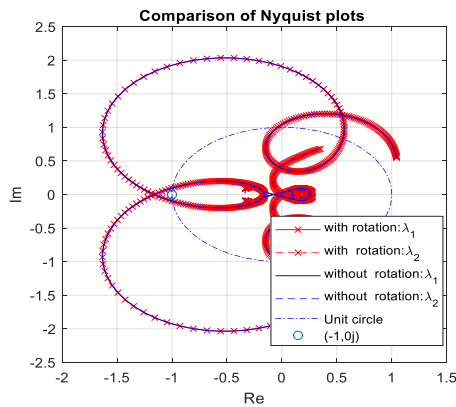
(b) Comparison of the Nyquist plots

Fig. 4 A special case that the rotation does not affect the stability ($P_{vsc1} = P_{vsc2}$ =1.0 p.u.; $Z_1 = Z_2 = 0.1$ j p.u ; $Z_s = 0.125$ j p.u; VSC1: CC = 400, PLL = 20 Hz, PQ = 20 Hz; VSC2: CC = 200, PLL = 10, PQ = 10)

However, it should be noted that the case study in Fig. 4 is not general; for general studies, the rotation should always be included since it will affect both the aggregated impedances and stability conclusions, more discussion will be shown later.

C. Properties and impacts of the impedance rotation on the AC/DC coupled systems

In this section, an AC/DC coupled system as shown in Fig. 5 (a) will be analyzed. Typically, the sending-end VSC of the HVDC-link imposes a constant voltage and frequency control (i.e. *V/f*), whereas the receiving-end VSC controls the dc voltage of the HVDC. In order to derive the rotation matrix in a more general way, the voltage angles e.g. $\theta_{1,2,3,hvdc1}$ are initially referred to an arbitrary common reference frame. Also, for compact representations of the HVDC-link, it is modeled as three-port modules [30], e.g. for the sending-VSC (AC currents flow into the VSC is positive, dc current flows into the dc-link is positive, see appendix for the models):

$$\begin{bmatrix} I_{p\_hvdc1}^{local}(s) \\ I_{n\_hvdc1}^{local}(s) \\ I_{dc\_hvdc1}(s) \end{bmatrix} = \begin{bmatrix} \mathbf{Y}_{pn\_hvdc1}^{local}(s) & \mathbf{a}_{2\times1}(s) \\ \mathbf{b}_{1\times2}(s) & Y_{dc\_hvdc1}(s) \end{bmatrix} \begin{bmatrix} U_{p\_hvdc1}^{local}(s) \\ U_{n\_hvdc1}^{local}(s) \\ U_{dc\_hvdc1}(s) \end{bmatrix} \quad (9)$$

where $\boldsymbol{I}_{pn\_hvdc1}^{local}$, $\boldsymbol{U}_{pn\_hvdc1}^{local}$ are local variables with respect to the *local reference frame* provided by $\angle\theta_{hvdc1}$.

Since the dc-side variables are irrelevant to reference frames, the AC/DC rotation matrix

$$\mathbf{T}_{rot\_hvdc}\left(\theta_{hvdc1}\right) = \begin{bmatrix} \mathbf{T}_{rot}\left(\theta_{hvdc1}\right) & \mathbf{0}_{2\times1} \\ \mathbf{0}_{1\times2} & 1 \end{bmatrix} \quad (10)$$

is obtained by modifying the AC one, e.g. $\boldsymbol{T}_{rot}(\theta_1)$. Applying this matrix on both sides of (9) yields:

$$\mathbf{Y}_{HVDC1}^{global} = \begin{bmatrix} \mathbf{T}_{rot}\left(-\theta_{hvdc1}\right)\mathbf{Y}_{pn\_hvdc1}^{local}\mathbf{T}_{rot}\left(\theta_{hvdc1}\right) & \mathbf{T}_{rot}^{hvdc}\left(-\theta_{hvdc1}\right)\mathbf{a}_{2\times1} \\ \mathbf{b}_{1\times2}\mathbf{T}_{rot}\left(\theta_{hvdc1}\right) & Y_{dc\_hvdc1} \end{bmatrix} \quad (11)$$

clearly, all the elements of the matrix are affected by this rotation matrix except the Y_{dc_hvdc1} .

Usually, when an AC/DC coupled system is analyzed, the ac-side impedance can be integrated to the dc-side by circuit operations. First, the aggregated admittance of the sending area (see Fig. 5 (a)) is written as

$$\mathbf{Y}_{pn\_pcc1}^{global} = \left(\mathbf{Z}_1 + \mathbf{T}_{rot}\left(-\theta_1\right)\mathbf{Z}_{pn\_vsc1}^{local}\mathbf{T}_{rot}\left(\theta_1\right)\right)^{-1} +$$
$$\left(\mathbf{Z}_1 + \mathbf{T}_{rot}\left(-\theta_2\right)\mathbf{Z}_{pn\_vsc2}^{local}\mathbf{T}_{rot}\left(\theta_2\right)\right)^{-1} \quad (12)$$

Then, substituting it into (11) yields

$$I_{dc\_hvdc1} = \left[\mathbf{b}_{1\times2}\left(\mathbf{Y}_{pn\_pcc1}^{local} - \mathbf{Y}_{pn\_hvdc1}^{local}\right)^{-1}\mathbf{a}_{2\times1} + Y_{dc\_hvdc1}\right] \cdot U_{dc\_hvdc1}$$
$$\rightarrow -I_{dc\_hvdc1} = Y_{dc\_port}^{hvdc1} \cdot U_{dc\_hvdc1} \quad (13)$$

where $\boldsymbol{Y}_{pn\_pcc1}^{local} = \boldsymbol{T}_{rot}(\theta_{hvdc1})\boldsymbol{Y}_{pn\_pcc1}^{global}\boldsymbol{T}_{rot}(-\theta_{hvdc1})$, it is noticed that the global admittance of the sending area (i.e. $\boldsymbol{Y}_{pn\_pcc1}^{global}$) is re-transformed into the local frame of the sending-VSC (i.e. $\angle\theta_{hvdc1}$).

Therefore, the *effective* global reference frame is actually the local reference frame of the sending-VSC (i.e. $\angle\theta_{hvdc1}$) rather than the arbitrary one as initially defined. This means, the *effective* rotation matrix for the *i*th ac-side impedance of the sending-area is $\boldsymbol{T}_{rot}(\theta_i - \theta_{hvdc1})$, which is obtained by expanidng $\boldsymbol{Y}_{pn\_pcc1}^{local}$ using (12).

Besides, if further include the dc side capacitor, the total dc-side admittance seen from the sending-end VSC is obtained

$$Y_{dc\_send}\left(s\right) = Y_{dc\_port}^{hvdc1}\left(s\right) + sC_{cap1} \quad (14)$$

For the receiving-end VSC's analysis, a similar process can be done, where the global reference frame can be initially chosen as the voltage angle of the Thevenin grid, i.e. $\angle\theta_s = 0$. Likewise, the three-port module of the receiving-VSC is written as (ac currents flow out of VSC is positive, dc current flows into the VSC is positive, see appendix for the models):
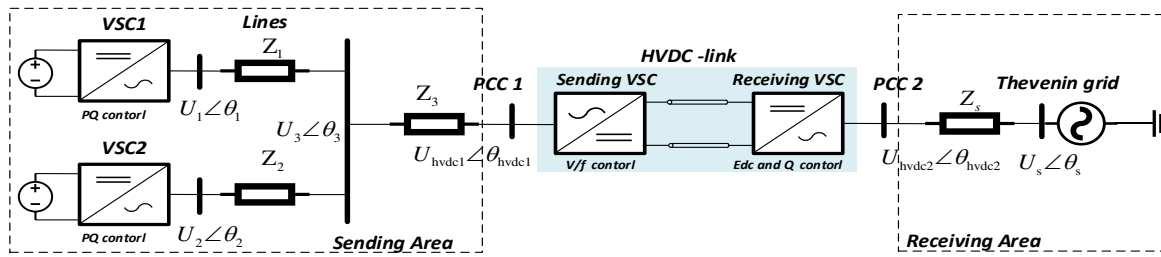
(a) Schematic of the AC/DC coupled system
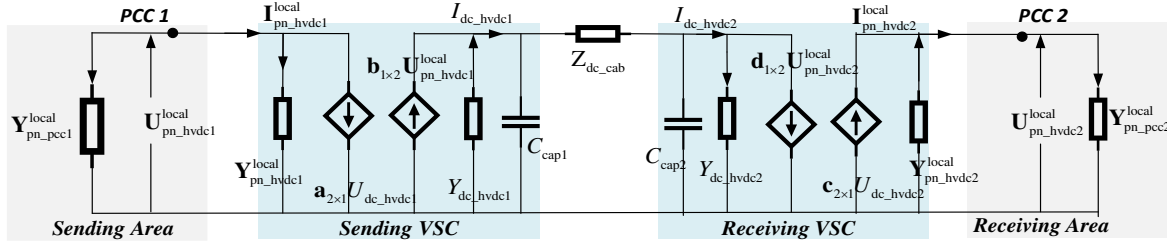
(b) Circuit representation of the AC/DC coupled system

Fig. 5 A simple interconnected AC/DC power electronics system for the study

$$\begin{bmatrix} I_{p\_hvdc2}^{local} \\ I_{n\_hvdc2}^{local} \\ I_{dc\_hvdc2} \end{bmatrix} = \begin{bmatrix} \mathbf{Y}_{pn\_hvdc2}^{local} & \mathbf{c}_{2\times1} \\ \mathbf{d}_{1\times2} & Y_{dc\_hvdc2} \end{bmatrix} \begin{bmatrix} U_{p\_hvdc2}^{local} \\ U_{n\_hvdc2}^{local} \\ U_{dc\_hvdc2} \end{bmatrix} \quad (15)$$

By introducing the global ac-side admittance of the receiving area (i.e. seen from PCC2) $\mathbf{Y}_{pn\_pcc2}^{global}$, the dc-side impedance of the receiving-end VSC is obtained as:

$$I_{dc\_hvdc2} = \left[\mathbf{d}_{1\times2} \left(\mathbf{Y}_{pn\_pcc2}^{local} - \mathbf{Y}_{pn\_hvdc2}^{local} \right)^{-1} \mathbf{c}_{2\times1} + Y_{dc\_hvdc2} \right] \cdot U_{dc\_hvdc2}$$
$$\rightarrow I_{dc\_hvdc2} = Y_{dc\_port}^{hvdc2} \cdot U_{dc\_hvdc2} \quad (16)$$

where $\mathbf{Y}_{pn\_pcc2}^{local} = \mathbf{T}_{rot}(\theta_{hvdc2}) \mathbf{Y}_{pn\_pcc2}^{global} \mathbf{T}_{rot}(-\theta_{hvdc2})$ is the admittance with respect to the local reference frame provided by $\angle\theta_{hvdc2}$.

Besides, if further includes the dc-side capacitor, the total dc-side admittance seen from the receiving-VSC is

$$Y_{dc\_rec}(s) = Y_{dc\_port}^{hvdc2}(s) + sC_{cap2} \quad (17)$$

Based on the above derivation, for the receiving-end VSC's analysis, the *effective* rotation matrix for the *j*th ac-side impedance within the sending-area is $\mathbf{T}_{rot}(\theta_j - \theta_{hvdc2})$, which is a similar result as the sending-end VSC's analysis.

In addition to the above dc-side analysis, the AC/DC coupled system can also be analyzed at one of the ac-side, for which the ac-side admittances seen from the sending- or the receiving-VSC can be derived, e.g. (18) and (19). For instance, if the analysis is at the ac-side of the sending-VSC, then the dc-side admittance/impedance of the opposite side (i.e. $Y_{dc\_rec}(s)$) is first developed in its own reference frame based on (16) and (17). Afterward, circuit analysis and operation are performed to derive the final ac-side admittance (18) for analysis. A similar process can be done for the ac-side of the receiving-VSC.

In summary, the HVDC decouples the ac systems in terms of reference frames. For each ac system, the ac impedances in that area should be transformed into a reference frame provided by the corresponding AC/DC interface, e.g. the sending- or receiving-VSC. Once it has been done, all the impedances are unified and they can be connected via basic circuit laws, the resulting circuit model is shown in Fig. 5 (b).
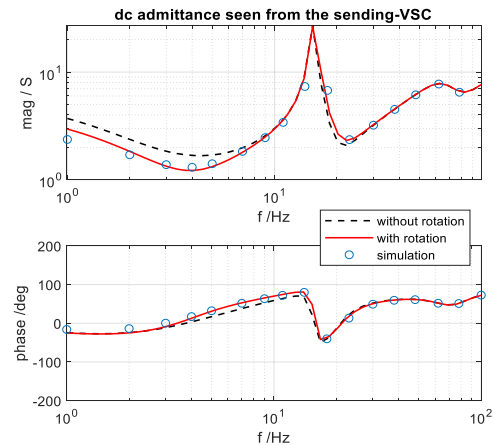
(a) The dc-side admittance seen from the sending-VSC
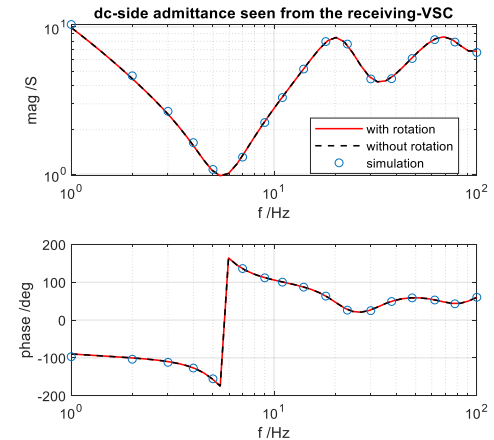
(b) The dc-side admittance seen from the receiving-VSC

Fig. 6 Impedance comparisons of the AC/DC coupled system with and without the rotation (for VSC1 and VSC2: PQ control = 10 Hz, PLL = 20 Hz, CC = 300 Hz, P = 1.0. p.u.; for VSC-HVDC, dc voltage control = 50 Hz, Q control = 10 Hz, PLL = 10 Hz, ac grid SCR = 4; $Z_1 = Z_2 = Z_3 = 0.1$ j p.u.; frequency is swept from 1 to 100 Hz in logarithmic

This article has been accepted for publication in a future issue of this journal, but has not been fully edited. Content may change prior to final publication. Citation information: DOI 10.1109/JESTPE.2019.2914560, IEEE Journal of Emerging and Selected Topics in Power Electronics

> REPLACE THIS LINE WITH YOUR PAPER IDENTIFICATION NUMBER (DOUBLE-CLICK HERE TO EDIT) <   6

To further illustrate this rotation effects, the dc-side admittances e.g. (14) and (17) are calculated with and without the rotation when using the circuit operations. And, they are compared with the simulated frequency-scanning results.

As shown in Fig. 6 (a) and (b), overall, the dc-side admittances with the rotation are consistent with simulations, whereas the ones without the rotation also exhibit some errors. Furthermore, it is noted that the dc-side admittance of the receiving-VSC seems not affected by the rotation, see Fig. 6 (b). This is because the receiving area of this study only contains a Thevenin equivalent grid, whose impedance is dq symmetric and thus is invariant in terms of the rotation (according to P.1). In general, the rotation will affect both the magnitude and phase response like the plots in Fig. 6 (a). Therefore, the accuracy of stability assessments will be affected as well if the rotation is not properly considered. This will be shown in the next case study, where the stability of the AC/DC coupled system is evaluated at the dc side via Nyquist plots.

The respective dc-side impedances (with the rotation) seen from the sending- and the receiving-VSC have been developed in (14) and (17), by further including the dc-side cable model, the dc-side source and load model (with the rotation) can be obtained and defined, e.g. the source impedance is $Z_{dc\_S}(s) = Y_{dc\_rec}^{-1}(s)$, and the load admittance is as $Y_{dc\_L}(s) = (Y_{dc\_send}^{-1}(s) + Z_{cab}(s))^{-1}$. On the other hand, the dc-side source and load model without the rotation can be derived similarly, where Z_{dc_S} and Y_{dc_L} are calculated without considering the rotation, i.e. all the ac impedances using the locally defined ones. After this, impedance-ratio (i.e. the minor loop gain) can be formulated, e.g. $L = Z_{dc\_S}Y_{dc\_L}$, then the Nyquist plots with and without the rotation can be compared.

It should be noted that before inspecting the Nyquist plots, the open-loop poles of the impedance-ratio should be evaluated to see if there are right-half-plane (RHP) poles. As discussed before, since the source impedance of this study is not affected by the rotation (see Fig. 6 (b)), only the poles of the load admittance with and without rotation are calculated. As shown in Fig. 7 (a), there is a pair of RHP pole in the source impedance, whereas the load admittance does not have any RHP poles. Based on this RHP poles evaluation and the Nyquist plots in Fig. 7 (b), it is obtained that without the rotation it concludes a stable system, whereas with the rotation it concludes an unstable system. Further, time domain simulation in Fig. 7 (c) proves that the stability conclusion without the rotation is incorrect. This case study clearly shows the importance of the rotation on accurate stability analysis.
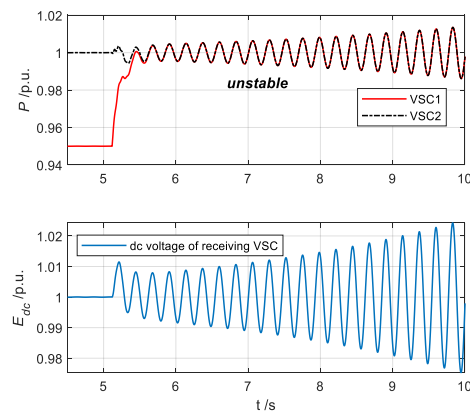
The above sections discuss the rotation operation and emphasize its importance in accurate impedance network
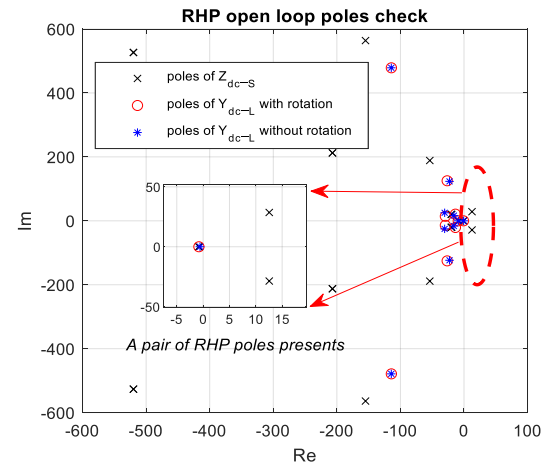
(a) Open-loop RHP poles check
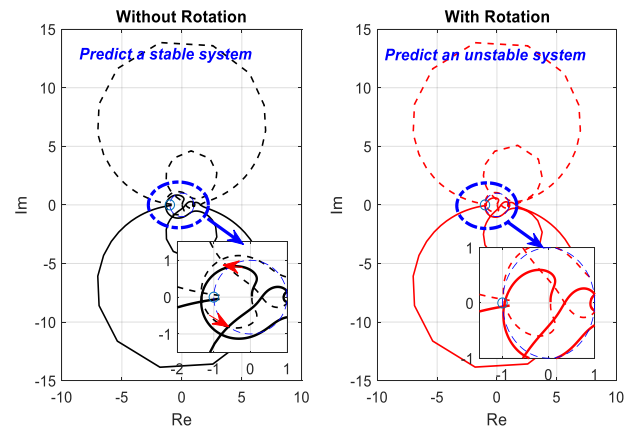
(b) Nyquist plots comparison

(c) Time domain simulation (a small step change of the active power reference is applied to VSC1)

Fig. 7 A case study of the stability effects of the rotation on the AC/DC coupled system (VSC1 and VSC2: PLL = 20 Hz, CC = 300 Hz, PQ = 10 Hz, output power = 1 p.u. VSC-HVDC receiving end: PLL = 20 Hz, dc voltage control = 45 Hz, reactive power control = 10 Hz, Z_1= Z_2= 0.1 j p.u. Z_3 = 0.1 j p.u., Z_s = 0.125 j p.u., Z_{dc_cab} = 0.05 j p.u.)

$$\begin{bmatrix} I_{p\_hvdc1}^{local}(s) \\ I_{n\_hvdc1}^{local}(s) \end{bmatrix} = \left(\mathbf{Y}_{pn\_hvdc1}^{local}(s) + \frac{\mathbf{a}_{2\times1}(s)\mathbf{b}_{1\times2}(s)}{\left(Y_{dc\_rec}^{-1}(s) + Z_{dc\_cab}(s)\right)^{-1} - Y_{dc\_hvdc1}(s)} \right) \begin{bmatrix} U_{p\_hvdc1}^{local}(s) \\ U_{n\_hvdc1}^{local}(s) \end{bmatrix} \qquad (18)$$

$$\begin{bmatrix} I_{p\_hvdc2}^{local}(s) \\ I_{n\_hvdc2}^{local}(s) \end{bmatrix} = \left(\mathbf{Y}_{pn\_hvdc2}^{local}(s) + \frac{\mathbf{c}_{2\times1}(s)\mathbf{d}_{1\times2}(s)}{\left(Y_{dc\_send}^{-1}(s) + Z_{dc\_cab}(s)\right)^{-1} - Y_{dc\_hvdc2}(s)} \right) \begin{bmatrix} U_{p\_hvdc2}^{local}(s) \\ U_{n\_hvdc2}^{local}(s) \end{bmatrix} \qquad (19)$$

(a) Norton admittance model for SC3   (b) Source and load model at PCC for SC1   (c) Closed-loop circuit for SC2
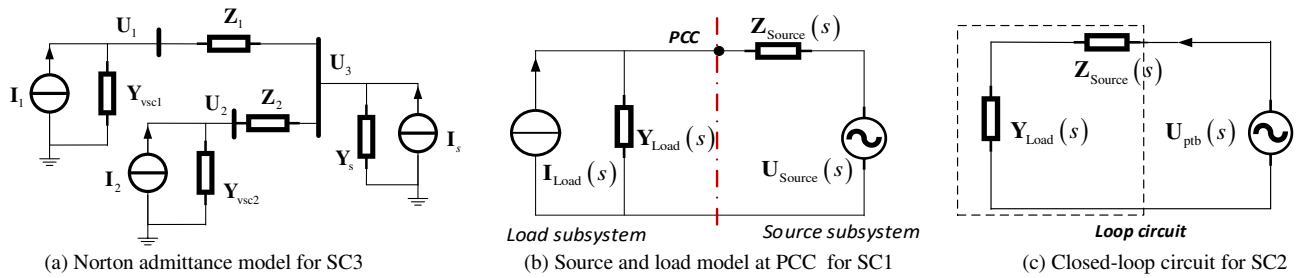
Fig. 8 Circuit representations of the AC coupled system for stability analysis

modeling and stability assessment. It lays the foundation for the forthcoming analyses, where the restrictions and conditions of different stability criteria when applied to impedance networks will be discussed. And, without special indication, all the impedance models will be calculated with the rotation.

III. COMPARATIVE STUDIES OF THE STABILITY CRITERIA FOR IMPEDANCE NETWORK STABILITY ASSESSMENTS

A. Overview of impedance-based stability criteria

Impedance-based stability criteria for either ac and dc systems have been extensively discussed before (e.g. [10] and [19]). Typically, for a single-VSC and grid system, a source and load equivalent system partitioned at the grid connection point can be established [20]; then the impedance-ratio (i.e. minor loop gain) of this equivalent system is analyzed and plotted in a complex plane (i.e. the eigenloci); afterward, by counting the number of encirclement of the eigenloci, overall stability of the equivalent system can be concluded according to the (inverse) Nyquist criterion [31], this method is referred to as the "Nyquist-based stability analysis" in this work. It has been noticed that, aside from the impedance-ratio, the source and load model can be formulated in different ways according to the control characteristics of converters, e.g. the "Z+Z" type and "Z+Y" as presented in [32], it claims that the typical impedance-ratio-based criterion may not be sufficient for this "Z+Z" type system, where the encirclement of the denominator impedance (a term in [32]) should also be counted. In fact, this modified criterion is related to the RHP poles issue of the impedance-ratio-based methods. And this RHP poles issue on accurately evaluating stability through the Nyquist criterion is further emphasized in [33] and [34]. In which, [33] shows that the RHP poles of multi-converter systems can be easily found due to interconnections and equivalents. Therefore, careful attention should be paid here if the Nyquist criterion and impedance-ratio are applied. Later, it will be shown that the Nyquist-based analysis is also sensitive to the partition points.

On the other hand, one way may avoid this RHP poles issue is to employ the closed-loop types of stability criteria, e.g., recent applications of wind farm analysis (e.g.[22]-[24]) show that the stability of an interconnected system can be evaluated by the *loop impedance* and the *Norton admittance*, which are all obtained from the impedance network model.

Since there are fundamental differences in applying those stability criteria of a single VSC and grid system to an interconnected one, a clarification on this regard is necessary.

To fulfill this task, comparative studies of stability criteria will be conducted in this section, from which several issues, e.g. the order-cancellation and the sensitivity to partition points, etc., are revealed and clarified. For a better presentation, those stability criteria aimed at comparing are briefly introduced.

B. Introduction of the three types of stability criteria

Once the rotation issue is addressed, impedance network of an interconnected system can be accurately formulated via basic circuit laws or systematically by the Norton admittance matrix, e.g., for the AC coupled system in Fig. 8 (a) it is

$$
\begin{bmatrix} \mathbf{I}_1(s) \\ \mathbf{I}_2(s) \\ \mathbf{I}_s(s) \end{bmatrix} = \underbrace{\begin{bmatrix} \underbrace{\begin{bmatrix} \mathbf{Y}_{vsc1} + \mathbf{Y}_1 & \mathbf{0}_{2\times 2} \\ \mathbf{0}_{2\times 2} & \mathbf{Y}_{vsc2} + \mathbf{Y}_2 \end{bmatrix}}_{\mathbf{Y}_{sys}^{sub1}} & \underbrace{\begin{bmatrix} -\mathbf{Y}_1 \\ -\mathbf{Y}_2 \end{bmatrix}}_{\mathbf{Y}_{sys}^{sub2}} \\ \underbrace{\begin{bmatrix} -\mathbf{Y}_1 & -\mathbf{Y}_2 \end{bmatrix}}_{\mathbf{Y}_{sys}^{sub3}} & \underbrace{\mathbf{Y}_1 + \mathbf{Y}_2 + \mathbf{Y}_s}_{\mathbf{Y}_{sys}^{sub4}} \end{bmatrix}}_{\mathbf{Y}_{sys}(s)} \begin{bmatrix} \mathbf{U}_1(s) \\ \mathbf{U}_2(s) \\ \mathbf{U}_3(s) \end{bmatrix} \quad (20)
$$

where $\mathbf{Y}_{vsc1}, \mathbf{Y}_{vsc1}$ are VSC1's and VSC2's MSD admittance, $\mathbf{Y}_1, \mathbf{Y}_2$ are the line admittances. $\mathbf{I}_s = \mathbf{Y}_s \mathbf{U}_s$ is the Norton equivalent of the ac grid. $\mathbf{I}_1, \mathbf{I}_2$ are the independent current sources of VSC1 and VSC2. It is noted that, since all the converters are designed to be stable under an ideal grid condition, thereby $\mathbf{I}_1, \mathbf{I}_2$ are stable (e.g. [20], [33]).

1) Nyquist-based stability analysis

For this criterion, a partition point is first defined for finding the source and load equivalents, usually, the PCC, see the equivalent system in Fig. 8 (b), where the source subsystem of this case is the grid impedance, which is $\mathbf{Z}_{Source} = \mathbf{Z}_s$, and the load subsystem is found from (20) by replacing the grid branch with an injection $\mathbf{I}_{inj}$, the resulting model is

$$
\begin{bmatrix} \mathbf{I}_1(s) \\ \mathbf{I}_2(s) \\ \mathbf{I}_{inj}(s) \end{bmatrix} = \begin{bmatrix} \mathbf{Y}_{sys}^{sub1} & \mathbf{Y}_{sys}^{sub2} \\ \mathbf{Y}_{sys}^{sub3} & \mathbf{Y}_{sys}^{sub4} - \mathbf{Y}_s \end{bmatrix} \begin{bmatrix} \mathbf{U}_1(s) \\ \mathbf{U}_2(s) \\ \mathbf{U}_3(s) \end{bmatrix} \quad (21)
$$

by setting $\mathbf{I}_1 = \mathbf{I}_2 = 0$

$$
\mathbf{I}_{inj}(s) = \underbrace{\left(\mathbf{Y}_{sys}^{sub4} - \mathbf{Y}_s - \mathbf{Y}_{sys}^{sub3} \left(\mathbf{Y}_{sys}^{sub1} \right)^{-1} \mathbf{Y}_{sys}^{sub2} \right)}_{\mathbf{Y}_{Load}(s)} \cdot \mathbf{U}_3(s) \quad (22)
$$

thus $\mathbf{Y}_{Load}$ is obtained and corresponding Norton current source is obtained from (21) by setting $\mathbf{U}_3 = \mathbf{0}$ and measuring $-\mathbf{I}_{inj}$, i.e. $\mathbf{I}_{Load} = -\mathbf{Y}_{sys}^{sub3}(\mathbf{Y}_{sys}^{sub1})^{-1} \begin{bmatrix} \mathbf{I}_1 \\ \mathbf{I}_2 \end{bmatrix} \mathbf{Y}_{Load}$.

(a) Nyquist plots at PCC　　　(b) zeros-plots of SC2 and SC3　　　(c) Time domain simulation
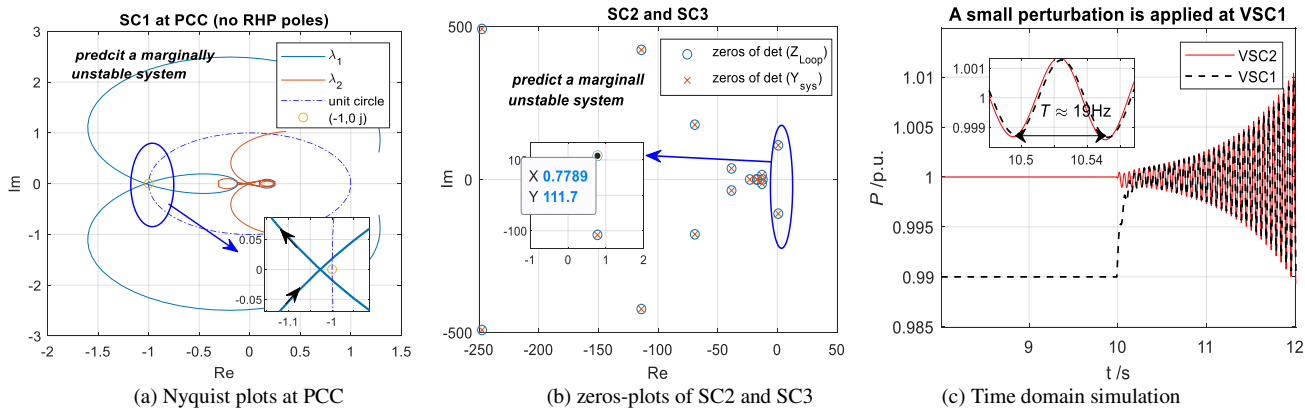
Fig. 9 Case I (VSC1-PLL = 15 Hz, VSC2-PLL = 40 Hz, others: PQ = 20 Hz, CC = 300 Hz, P = 1.0 p.u.; $Z_1 = Z_2 = 0.1$ j p.u., $Z_s = 0.125$ p.u.)

Consequently, the impedance-ratio is derived as $L_{AC} = Z_{Source}L_{Load}$ and based on which the Nyquist criterion states:

Stability criterion 1(SC1): if L_{AC} does not contain any right RHP poles, then the closed-loop system is stable if and only if the eigen-loci of L_{AC} does not encircle the critical point (-1, 0 j). If L_{AC} has RHP poles, the system is stable if and only if the number of counterclockwise encirclements of the (-1,0 j) equals to the number of the RHP poles of L_{AC}, otherwise, it is unstable.

Remark: Since the impedance-ratio is essentially an equivalent model derived from circuit operations on the impedance network, improper circuit operations (e.g. operation on identical branches) may result in inaccurate equivalent models and stability conclusions. On the other hand, physically, the impedance-ratio can be regarded as a metric of the interactive stability of two subsystems at a given point, and the intensity of this interaction could vary if a different partition point is inspected. This feature, in this work, is referred to as the "sensitivity to partition points" that will be explored later.

2) Loop impedance-based stability analysis

As noticed before, the loop impedance is a closed-loop model of an impedance network, characterizing the system's response seen from one point, see Fig. 8 (c), the loop impedance is

$$\mathbf{Z}_{Loop}(s) = \mathbf{Y}_{Load}^{-1}(s) + \mathbf{Z}_{Source}(s)$$
$$= (\mathbf{Z}_1 + \mathbf{Z}_{vsc1})\|(\mathbf{Z}_2 + \mathbf{Z}_{vsc2}) + \mathbf{Z}_s \quad (23)$$

where $\mathbf{Z}_{vsc1,2} = \mathbf{Y}_{vsc1,2}^{-1}$, $\mathbf{Z}_{1,2} = \mathbf{Y}_{1,2}^{-1}$, and $\mathbf{Z}_s = \mathbf{Y}_s^{-1}$.

Based on the circuit properties, the current response is stable if $\mathbf{Y}_{Loop}$ does not have any RHP poles. Since $\mathbf{Y}_{Loop} = \mathbf{Z}_{Loop}^{-1} = \frac{adj(\mathbf{Z}_{Loop})}{\det(\mathbf{Z}_{Loop})}$, this stability criterion can be stated as:

Stability Criterion 2 (SC2): The closed-loop system is stable if and only if there are no RHP poles of $\mathbf{Y}_{Loop}$, or equivalently there are no RHP zeros of $\det(\mathbf{Z}_{Loop})$.

Remark: Compared to the impedance-ratio of SC1, this criterion employs a model resembling the impedance-sum. However, the stability criterion is different, where SC2 directly evaluates the stability through the closed-loop poles. Therefore, SC2 is absent of the RHP poles issue. Nevertheless, since the loop impedance is derived by imposing the circuit

operations on the impedance network, it is an equivalent model that is sensitive to improper circuit operations as well.

3) Norton admittance-based stability analysis

Rather than using the equivalents, the Norton admittance (20) can be directly employed for stability analysis. Since the Norton admittance is obtained through current injections, the voltage responses are stable if $\mathbf{Z}_{sys}$ does not have any RHP poles. Also, due to $\mathbf{Z}_{sys} = \mathbf{Y}_{sys}^{-1} = \frac{adj(\mathbf{Y}_{sys})}{\det(\mathbf{Y}_{sys})}$, this criterion can be stated as:

Stability Criterion 3 (SC3): The closed-loop system is stable if and only if there are no RHP poles of $\mathbf{Z}_{sys}$, or equivalently there are no RHP zeros of $\det(\mathbf{Y}_{sys})$.

Remark: Clearly, the Norton admittance model preserves the overall system's structure, therefore it is less sensitive to the circuit operations compared to SC1 and SC2. Also, it is a closed-loop type of criterion since it calculates and evaluates all the closed-loop poles of the system directly.

C. Comparative studies of SC1, SC2, and SC3 on stability

This section selects the AC coupled system (e.g. Fig. 2) for the analysis. Notice that all the models are accurately derived with the rotation, thus stability impacts are only associated with the stability criteria aimed at comparing.

1) Case I: A case to show the consistency of SC1-SC3

First, a marginally unstable case is selected (known as the critical case) to show the model accuracy and the consistency of those criteria in stability assessments.

As shown in Fig. 9 (a), the Nyquist plot (SC1) predicts an unstable system, more specifically, a marginally unstable system since the clockwise encirclement is close to the critical point (-1,0 j). In Fig. 9 (b), a similar conclusion is drawn according to the results of SC2 and SC3, where a pair of RHP zeros close to the imaginary axis is presented. To justify the stability predictions of SC1, SC2, and SC3, time domain simulation with a small perturbation applied to the VSC1 is shown in Fig. 9 (c). From which it is seen that the system is indeed a marginally unstable one. Besides, the oscillation frequency of the active power is around 19 Hz, which is close to the predicted frequency of SC2 and SC3, i.e. $\frac{111.7}{2\pi} \approx 18.6$ Hz, this again justifies the model accuracy.
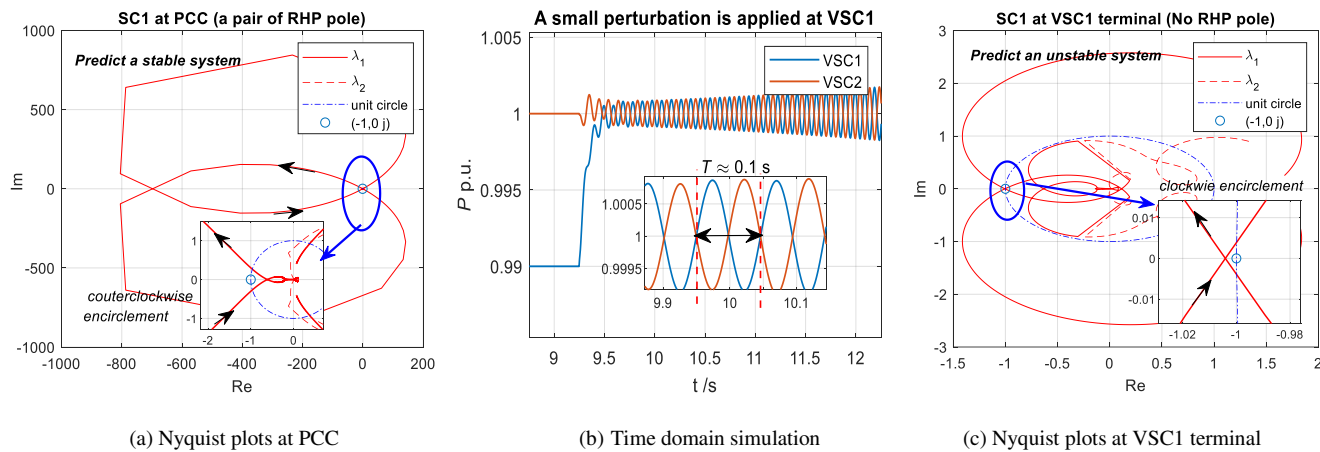
(a) Nyquist plots at PCC   (b) Time domain simulation   (c) Nyquist plots at VSC1 terminal

Fig. 10 Case II (VSC1 and VSC2 are identical: CC = 150 Hz, PLL = 20 Hz, PQ = 10 Hz, P = 1.0 p.u.; $Z_1 = Z_2$ = 0.15 j p.u.; Z_s = 0.15 p.u., in this case the grid impedance is pure resistive to better show this effect)

The above case study shows that for general studies those criteria seem consistent, however, there does exist some special cases where the inconsistency may occur. This is because the models of SC1 and SC2 are derived from circuit equivalents, thus conveying some restrictions, e.g. sensitive to circuit operations as mentioned before.

2) Case II: A case to show the inconsistency of SC1-SC3

To provoke the issue of concern, the same study system, however, with the presence of identical branches is constructed. This is fulfilled by imposing the condition: $Y_{vsc1} = Y_{vsc2}$ and $Z_1 = Z_2$. As a result, the "order-cancellation" issue will be unintentionally provoked (see appendix. C for more illustration), and it will affect the models of SC1 and SC2 since they are derived from circuit equivalents. For example, the impedance of the load branch under such a condition is simplified to $Z_{Load} = 0.5 \cdot (Z_{vsc1} + Z_1)$, clearly, the order of which is reduced by *half*.

Table I ZEROS OF SC2 AND SC3 UNDER CASE II

SC2 (*10^2)	SC3(*10^2)	
Zeros of det (Z_{Loop}) (*10^2)	Zeros of det (Y_{sys}) (*10^2)	
-0.1298 + 0.0132i	-0.1088 - 0.0142i	-0.0367 + 0.3796i
-0.1298 - 0.0132i	-0.1088 + 0.0142i	-0.0367 - 0.3796i
-0.2115 - 0.1411i	-0.1298 + 0.0132i	**0.0004 + 0.6515i**
-0.2115 + 0.1411i	-0.1298 - 0.0132i	**0.0004 - 0.6515i**
-0.0367 + 0.3796i	-0.2115 - 0.1411i	-1.1954 + 3.7302i
-0.0367 - 0.3796i	-0.2115 + 0.1411i	-1.1954 - 3.7302i
-4.9087 + 3.3301i	-0.2131 - 0.1713i	-4.9087 + 3.3301i
-4.9087 - 3.3301i	-0.2131 + 0.1713i	-4.9087 - 3.3301i
Predict a **stable** system	Predict an **unstable** system	

To show its stability impacts, SC2 and SC3 are first compared in Table I. From which it is seen that SC2 loses half of the modes compared to SC3, more importantly, one of the missing modes is unstable (e.g. 0.04 ± 65.15 j), thus the SC2 will draw an opposite stability conclusion as the SC3. Next, the stability result of SC1 evaluated at the PCC is further shown in Fig. 10 (a), it is seen that the number of counterclockwise encirclements is the same as the number of the RHP poles (the evaluation is omitted), thus SC1 concludes a stable system.

Based on the stability tests, so far, SC1 and SC2 predict a stable system whereas SC3 predict an unstable one. To show which stability criterion is correct, time domain simulation with a small perturbation on VSC1 is conducted and the results are shown in Fig. 10 (b), clearly, it is a small-signal unstable system. Therefore, only SC3 succeeds in this stability test.

This comparison clearly reveals that the improper circuit operations (e.g. the order-cancellation) may result in inaccurate models for stability analysis, and finally leads to inaccurate stability assessments. This issue mostly affects the stability criteria using equivalent models e.g. SC1 and SC2, thus careful attention should be paid on that.

To address this issue, one could 1) calculate a new loop impedance defined at a different branch for SC2; and 2) define a new partition point and calculate the new source and load equivalent for SC1. For the former one, a simple justification is shown in the appendix. D; for the latter one, the Nyquist plot is re-evaluated at VSC1(the terminal of which is the new partition point) and shown in Fig. 10(c), since there are no RHP poles, the clockwise encirclements of (-1,0 j) indicate an unstable system, which is the correct conclusion as identified before.

Besides, from Fig. 10 (b) one may observe that the VSC1 and VSC2 within the identical branch are oscillating against each other (see the opposite phase of active power), which implies that this oscillation cannot be seen by the grid. This physically explains why the modes from SC2 are all stable.

Lastly, by comparing the Nyquist plots of different partition points (i.e. at PCC and VSC1), it is identified that SC1 is "sensitive to partition points", thus a stable conclusion of one partition point is merely a necessary but not sufficient condition for a stable system. Therefore, a scanning of all the partition points (i.e. multiple Nyquist plots) is suggested to assure a precise stability conclusion. Although this process complicates the stability assessments of SC1, it could be an advantage in identifying the system's weak point that will be presented in the next section. Besides, a brief summary of SC1, SC2, and SC3 on stability analysis is shown in Table II.
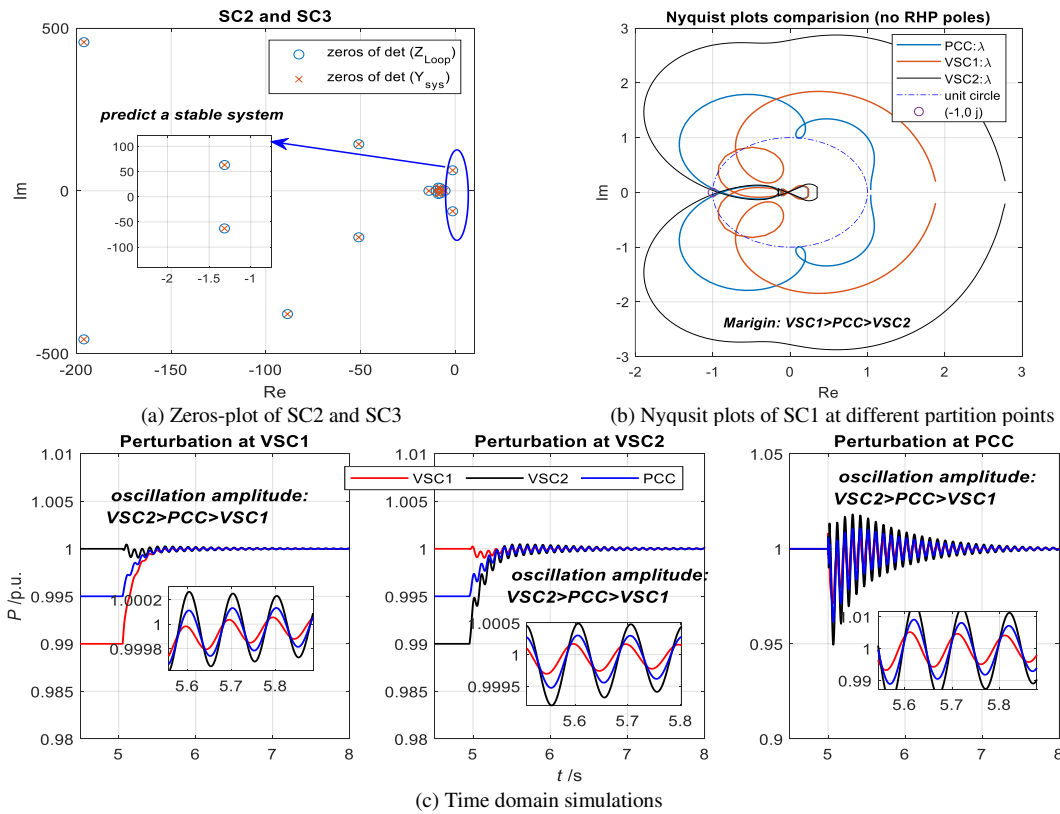
(a) Zeros-plot of SC2 and SC3

(b) Nyqusit plots of SC1 at different partition points

(c) Time domain simulations

Fig. 11 Nyquist-based analysis of system's weak point (VSC1: CC = 300 Hz, PLL = 10 Hz, PQ = 10 Hz, P = 1.0 p.u.; VSC2: CC = 220 Hz, PLL = 10 Hz, PQ = 10 Hz, P = 1.0 p.u; Z_1 = 0.1 j, Z_2 = 0.2 j p.u., Z_s = 0.125 j p.u.)

IV. DISCUSSION ON THE SYSTEM'S WEAK POINT IDENTIFICATION AND ITS APPLICATION TO THE NETWORK DESIGN AND PLANNING

A. Identification of the system's weak point

This section will analyze the AC coupled system under a stable condition. By scanning the partition points, multiple Nyquist plots can be obtained, from which the relative stability margins of each partition point can be extracted and compared so that the relative weak point is found.

First, stability predictions of SC2 and SC3 are shown in Fig. 11 (a). Since there are no identical branches of this study, it will be absent of the order-cancellation issue as encountered in a previous case study, thus the number of zeros of SC2 and SC3 under this case is identical, and they all predict a stable system.

Then, a scanning of partition points with SC1 will be performed. Before this, the source and load equivalents partitioned at the VSC1's and VSC2's terminal can be derived in a similar way as the one at the PCC (see Fig. 8 (b)). After this, multiple Nyquist plots are obtained and compared in Fig. 11 (b). Notice that, in this study, there are no RHP poles at those partition points, meanwhile, only the dominant eigenloci are shown. From the multi-Nyquist plots, it is seen that the partition point at VSC1 exhibits the highest relative margin, followed by the one at the PCC, whereas the partition point at the VSC2 has the lowest relative margin. Therefore, the partition point at the VSC2's terminal is the identified vulnerable point.

To verify if this identified weak point is correct or not, small perturbations at VSC1, VSC2, and PCC are applied respectively to provoke the small-signal dynamics from different parts of the system. In which, perturbations at VSC1 and VSC2 are fulfilled by a small change of active power reference (i.e. 0.01p.u.), whereas the perturbation at PCC is fulfilled by a small magnitude change of grid voltage (i.e. 0.01p.u.). The results are shown in Fig. 11 (c), it is seen that regardless of the location of the perturbations, the VSC2 always exhibits the most intensive oscillatory behavior, indicating it is the system's weak point.

In summary, this study successfully shows the capability of the Nyquist-based analysis in the identification of the system's weak point. This knowledge is useful for the network design and planning if new components are going to be connected, this benefit will be shown in the next case study.

B. Stability-oriented network design and planning

This section will show how the knowledge of identified weak point can help the network planning from the stability point of view if a new VSC is going to be connected. A same study system as the previous one is employed, and the schematic diagram is shown in Fig. 12 (a), where the node U_2 is the identified weak point as the last case study has shown, and VSC3 is the new component going to be connected. To show the effects, simulations of two choices for placing VSC3 are compared, i.e. connected to U_1 (i.e. choice 1) and connected to U_2 (choice 2).
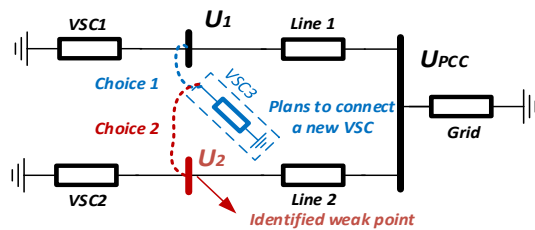
(a) Schematic diagram of adding a new VSC to the existing system
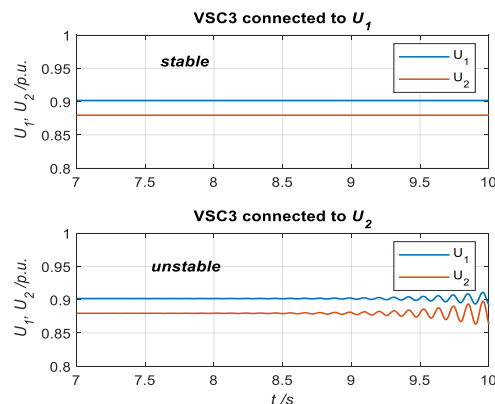
(b) Time domain simulations

Fig. 12 A case study on better network planning with the knowledge of identified weak point (VSC3: $PQ_{ref} = 0$ p.u. since the control impacts are focused. PQ = 10 Hz, PLL = 10 Hz, CC = 500 Hz. Configurations of the rests are identical to Fig. 11)

In the simulation, before the VSC3 is connected, the current controller of VSC2 is initially set to 300 Hz to assure a good overall margin. After the VSC3 is connected and the system is in steady state (around 7 s), the current controller of VSC2 is then reduced to 220 Hz (a value used in Fig. 11). Based on this process, simulation results are shown in Fig. 12 (b). It is clearly observed that if VSC3 is connected to the node U_1, the resulting system is still stable; whereas if it is connected to the node U_2, the resulting system is unstable. The mechanism behinds this is clear, which is due to the fact that the node U_2 is the identified

weak point (i.e. Fig. 11) of the system, thus it is susceptible to be unstable when new components are connected here. Therefore, from a stability-oriented network planning point of view, the node U_1 is the preferable place for adding new components.

V. CONCLUSION

Impedance is a linear concept with clear physical implications. Typically, the impedance of a VSC is locally evaluated via linearization, a process which is dependent on the reference frame where the linearization is performed, thus an operation of matrix rotation is required before connecting them in circuits for the purpose of network stability analysis. This paper revealed three major properties associated with the rotation, and the rotation impacts on stability assessments are analyzed and clarified. It turns out that under a certain condition the rotation though will affect the shapes of an aggregated impedance, it may not affect the corresponding stability conclusion; however, the condition justifying the above statement is not general, also may not be useful from a practical viewpoint since it imposes a condition on all the VSCs that they should have identical load angles. Therefore, for the purpose of general and precise impedance network modeling and stability analysis, the operation of rotation should always be included.

On the other hand, even if the rotation operation is properly applied when formulating the impedance network, still, stability assessments of the impedance network may not be accurate if directly applying the stability criteria of a single VSC and grid system to an interconnected one. In this regard, three types of commonly employed stability criteria are compared and clarified regarding their restrictions and conditions, the major findings are:

1) The Nyquist-based (SC1) and the loop impedance-based (SC2) criteria are sensitive to circuit operations. Improper circuit operations, e.g. parallel operation on identical branches, may lead to wrong stability conclusions (i.e. the order-cancellation issue discussed in this work). The Norton

Table II A SUMMARY OF SC1, SC2, SC3 ON STABILITY ANALYSIS

Items	SC1	SC2	SC3
Description	Open-loop model resulting from circuit operation and equivalent i.e. Impedance-ratio	Closed-loop model resulting from circuit operation and equivalent i.e. Loop impedance	Closed-loop model with overall system structure i.e. Norton admittance
Stability criterion	Nyquist criterion	Zeros of det (Z_{Loop})	Zeros of det (Y_{sys})
Need RHP open-loop poles check?	Yes	No	No
Need or sensitive to partition point?	Yes	No	No
Need or sensitive to circuit operations?	Yes	Yes	No
Able to identify the system's weak point?	Yes	No	Could be (need further analysis)
Summary and Remarks	1) A stable conclusion of one partition point is only a necessary but not sufficient condition of a stable system (e.g. Case II); 2) A scanning of partition points (i.e. multi-Nyquist plots) is suggested to draw a precise stability conclusion locate system's vulnerable points.	1) Sensitive to circuit operations (e.g. the order cancellation issue in Case II may lead to inaccurate stability predictions); 2) One way may address this issue is to re-calculate the loop impedance from another branch and evaluate the stability.	1) In this work, SC3 exhibits fewer restrictions than SC1 and SC2 with respect to circuit operations; 2) Although its capability in weak point identification is not discussed in this work, there is a possibility to associate the vulnerable modes from the branch and node information.

admittance-based criterion (SC3) exhibits fewer restrictions on this regard since it preserves the overall system structure;

2) In addition to the above issue, stability analysis with SC1 is also sensitive to the partition points. It turns out that a stable conclusion of one partition points is merely a necessary but not sufficient condition for a stable system;

3) Countermeasures to address the above issues could be performing a scanning of partition points for SC1 (i.e. multiple Nyquist plots evaluation), and re-calculating the loop impedances from a different branch for SC2.

4) Specific to SC1, although the partition-points-scanning complicates the stability assessments, the process and the result of which is proven to be an advantage in identifying the system's weak point. Also, a further case study shows that this knowledge of the system's weak point can better facilitate the stability-oriented network design and planning when now components are going to be connected to the existing system, and in turn, making it a promising counterpart to the sensitivity analysis of the state-space models.

Lastly, in this work, SC3 exhibits fewer restrictions than SC1 and SC2 with respect to circuit operations, this does not necessarily imply that SC3 is a general criterion on all aspects. Its generality, as well as the capability in system's weak point identification, are worth being explored in future works.

APPENDIX

Appendix A and B will present the MSD employed for the analysis of the AC coupled and the AC/DC coupled system. Generally, they can be linearly transformed from the well-known dq impedances. One may refer to [11] for the dq impedance modeling, [17] for the concept and method of MSD impedance, and [18] for the MSD impedance modeling of control blocks. Overall, VSCs of this work are controlled with, i.e. the PQ, the E_{dc}/Q, and the V/f control.

A. MSD Impedance model of the PQ controlled VSC

The MSD admittance model of VSC1,2 is derived as:

$$Y^{local}_{pn\_vsc1,2} =$$
$$\begin{bmatrix} H_c\left(1 + 1.5U_{g0}^*H_s\right) + Z_{fp} & 0 \\ 0 & H_c\left(1 + 1.5U_{g0}H_s\right) + Z_{fp} \end{bmatrix}^{-1} \cdot$$
$$\begin{bmatrix} 1 - G_{pllp} & G_{pllp} + 1.5H_sH_cI_{c0} \\ G_{plln} + 1.5H_sH_cI_{c0}^* & 1 - G_{plln} \end{bmatrix} \quad (A.1)$$

where $G_{pllp} = \frac{0.5(U_{c0}+H_cI_{c0})H_{pll}}{s+U_{gd0}H_{pll}}$. H_c, H_s are the PI controllers for PLL and PQ control. $Z_{fp} = (s + j\omega_s)L_f + R_f$. $Z_{fp}(s) = (Z_{fn}(-s))^*$ and $G_{plln}(s) = (G_{pllp}(-s))^*$. U_{c0}, I_{c0} are the voltage and current phasors of VSC. U_{gd0} is d-axis grid voltage.

B. MSD Impedance model of HVDC-link (V/f and E_{dc}/Q)

The VSCs of the HVDC are represented by three-port modules. Here only presents the models within the modules.

1) The sending-end VSC (i.e. the V/f controlled VSC)

$$Y^{local}_{pn\_hvdc1} = \begin{bmatrix} Z_{hvdc\_fp} & 0 \\ 0 & Z_{hvdc\_fn} \end{bmatrix}^{-1} \cdot$$
$$\begin{bmatrix} 1 + 0.5e^{-j\theta_0}V^{hvdc}_{dc0}H_v & 0.5e^{-j\theta_0}V^{hvdc}_{dc0}H_v \\ 0.5e^{j\theta_0}V^{hvdc}_{dc0}H_v & 1 + 0.5e^{j\theta_0}V^{hvdc}_{dc0}H_v \end{bmatrix};$$
$$a_{2\times1} = \begin{bmatrix} \frac{0.5D_0^*e^{-j\theta_0}}{Z_{hvdc\_fp}} & \frac{0.5D_0e^{j\theta_0}}{Z_{hvdc\_fn}} \end{bmatrix}^T;$$
$$Y_{dc\_hvdc1} = 1.5 \cdot [D_0e^{j\theta_0} \quad D_0^*e^{-j\theta_0}] \cdot a_{2\times1};$$
$$b_{1\times2} = 1.5 \cdot [D_0e^{j\theta_0} \quad D_0^*e^{-j\theta_0}] \cdot Y^{local}_{pn\_hvdc1} - 1.5 \cdot$$
$$H_vRe(I_{c0}e^{j\theta_0})\begin{bmatrix} 1 \\ 1 \end{bmatrix}^T \quad (A.2)$$

where H_v is the ac voltage PI controller, $Z_{hvdc\_fp} = (s + j\omega_s)L_{hvdc\_f} + R_{hvdc\_f}$. D_0 is the normalized ac voltage phasor of sending-VSC. I_{0_hvdc1} is the current phasor. θ_0 is the voltage angle between the PCC1 and the sending-VSC terminal. V^{hvdc}_{dc0} is the nominal dc voltage.

2) The receiving-end VSC (i.e. the Edc/Q controlled VSC)

$$Y^{local}_{pn\_hvdc2} = A(s)^{-1}B(s);$$
$$c_{2\times1} = A(s)^{-1}\begin{bmatrix} H_{dc}H_cV^{hvdc}_{dc0} + D_0 \\ H_{dc}H_cV^{hvdc}_{dc0} + D_0^* \end{bmatrix};$$
$$d_{1\times2} = \frac{1.5}{V^{hvdc}_{dc0}} \cdot [I_{0\_hvdc}^* \quad I_{0\_hvdc}] - \frac{3}{2} \cdot$$
$$\begin{bmatrix} \frac{I_{0\_hvdc}^*Z_{hvdc\_fp}}{V^{hvdc}_{dc0}} + D_0^* & \frac{I_{0\_hvdc}Z_{hvdc\_fn}}{V^{hvdc}_{dc0}} + D_0 \end{bmatrix} \cdot Y^{local}_{pn\_hvdc2};$$
$$Y_{dc\_hvdc2} = -\frac{1.5}{V^{hvdc}_{dc0}} \cdot$$
$$\begin{bmatrix} \frac{I_{0\_hvdc}^*Z_{hvdc\_fp}}{V^{hvdc}_{dc0}} + D_0^* & \frac{I_{0\_hvdc}Z_{hvdc\_fn}}{V^{hvdc}_{dc0}} + D_0 \end{bmatrix} \cdot c_{2\times1} - \frac{P_0}{(V^{hvdc}_{dc0})^2}$$
$$(A.3)$$

where
$$A(s) =$$
$$\begin{bmatrix} H_c \cdot \left(1 + \frac{3H_Q}{4}U_{g0\_hvdc}^*\right) + Z_{hvdc_{fp}} & -\frac{3H_QH_c}{4}U_{g0\_hvdc} \\ -\frac{3H_QH_c}{4}U_{g0\_hvdc}^* & H_c \cdot \left(1 + \frac{3H_Q}{4}U_{g0\_hvdc}\right) + Z_{hvdc\_fn} \end{bmatrix};$$
$$B(s) = \begin{bmatrix} 1 - G_{pllp} - \frac{3H_QH_c}{4}I_{0\_hvdc}^* & G_{pllp} + \frac{3H_QH_c}{4}I_{0\_hvdc} \\ G_{plln} + \frac{3H_QH_c}{4}I_{0\_hvdc}^* & 1 - G_{plln} - \frac{3H_QH_c}{4}I_{0\_hvdc} \end{bmatrix};$$

$G_{pllp} = \frac{0.5(D_0V^{hvdc}_{dc0}+H_cI_{0\_hvdc})H_{pll}}{s+U_{gd0\_hvdc}H_{pll}}$. H_c, H_{dc}, H_Q, are the current, dc voltage and reactive power PI controller. U_{gd0_hvdc} d-axis PCC2 voltage phasor. $D_0, I_{0\_hvdc}, V^{hvdc}_{dc0}$ have the same meaning as the sending-VSC. In addition, the dc cable is modeled as: $Z_{dc\_cab} = sL_{cab} + R_{cab}$.

C. Illustration of the order-cancellation issue

The loop impedance of the AC coupled system can be derived as, $Z_{Loop} = (Z_{BR1}^{-1} + Z_{BR2}^{-1})^{-1} + Z_s$, where $Z_{BR1} = Z_{vsc1} + Z_1$, and $Z_{BR2} = Z_{vsc2} + Z_2$. For better illustration, taking a scalar circuit as an example, where the loop impedance is simplified as $Z_{Loop} = \frac{Z_{BR1} \cdot Z_{BR2}}{Z_{BR1}+Z_{BR2}} + Z_s$, if the branch impedances are presented as polynomials and they are identical, then the loop impedance is written as

$$Z_{Loop} = \frac{\left(\frac{N_{BR1}(s)}{D_{BR1}(s)}\right)^2}{2\frac{N_{BR1}(s)}{D_{BR1}(s)}} + \frac{N_{BR_S}(s)}{D_{BR1}s(s)} \quad (A.4)$$

It is noted that, for SC2, zeros of Z_{Loop} determine the stability (i.e. the numerator). If the impedance of such parallel-connected branch in (A.4) are canceled ahead of deriving the total numerator, it will lead to a wrong numerator

$$N_{cancel} = N_{BR1}(s)D_s(s) + 2D_{BR1}(s)N_s(s) \quad (A.5)$$

whereas the correct one should be:

$$N_{correct} = N_{BR1}(s)N_{cancel}(s) \quad (A.6)$$

Clearly, the modes from $N_{BR1}(s)$ characterizing the parallel branch are lost.

D. *A simple way for addressing the order-cancellation issue*

To avoid the order-cancellation issue, one may calculate the loop impedance from another non-identical parallel branch, e.g. from BR1, the parallel branch will be $Z_s||Z_{BR2}$. Since Z_s is not identical to Z_{BR2}, the order-cancellation issue will not present. It is seen from the new loop impedance:

$$Z_{Loop} = Z_{BR1} + \frac{Z_{BR2}Z_s}{Z_s+Z_{BR2}} \quad (A.7)$$

By substituting the numerators and denominators, the numerator of this new loop impedance is:

$$N_{new} = N_{BR1}(s)(N_{BR1}(s)D_s(s) + 2D_{BR1}(s)N_s(s)) \quad (A.8)$$

which is the same as (A.6), i.e. $N_{new} = N_{correct}$. As a result, the order-cancellation issue is mitigated, however, to achieve this, prior knowledge of the branches is required.

REFERENCES

[1]. R. Teodorescu, M. Liserre, and P. Rodriguez, "Introduction," in Grid converters for photovoltaic and wind power systems, Chichester, United Kingdom: John Wiley & Sons, 2011, pp. 1–4.

[2]. N. Flourentzou, V. G. Agelidis and G. D. Demetriades, "VSC-Based HVDC Power Transmission Systems: An Overview," in IEEE Transactions on Power Electronics, vol. 24, no. 3, pp. 592-602, March 2009.

[3]. J. M. Guerrero, M. Chandorkar, T. Lee and P. C. Loh, "Advanced Control Architectures for Intelligent Microgrids—Part I: Decentralized and Hierarchical Control," in *IEEE Transactions on Industrial Electronics*, vol. 60, no. 4, pp. 1254-1262, April 2013.

[4]. L. P. Kunjumuhammed, B. C. Pal, C. Oates and K. J. Dyke, "Electrical Oscillations in Wind Farm Systems: Analysis and Insight Based on Detailed Modeling," in IEEE Transactions on Sustainable Energy, vol. 7, no. 1, pp. 51-62, Jan. 2016.

[5]. H. Liu, X.X. Xie, J.B. He, T. Xu, Z. Yu, C. Wang, C.Y. Zhang, "Subsynchronous Interaction Between Direct-Drive PMSG Based Wind Farms and Weak AC Networks," in IEEE Transactions on Power Systems, vol. 32, no. 6, pp. 4708-4720, Nov. 2017.

[6]. C. Li, "Unstable Operation of Photovoltaic Inverter From Field Experiences," in IEEE Transactions on Power Delivery, vol. 33, no. 2, pp. 1013-1015, April. 2018.

[7]. L. Fan, C. Zhu, Z. Miao and M. Hu, "Modal Analysis of a DFIG-Based Wind Farm Interfaced With a Series Compensated Network," in *IEEE Transactions on Energy Conversion*, vol. 26, no. 4, pp. 1010-1020, Dec. 2011.

[8]. M. Raza, E. Prieto-Araujo and O. Gomis-Bellmunt, "Small-Signal Stability Analysis of Offshore AC Network Having Multiple VSC-HVDC Systems," in *IEEE Transactions on Power Delivery*, vol. 33, no. 2, pp. 830-839, April 2018.

[9]. X. Wang and F. Blaabjerg, "Harmonic Stability in Power Electronic Based Power Systems: Concept, Modeling, and Analysis," in *IEEE Transactions on Smart Grid.* doi: 10.1109/TSG.2018.2812712 *(online)*.

[10]. Belkhayat M, "Stability criteria for AC power systems with regulated loads," Ph.D. dissertation, Purdue University, USA, 1997.

[11]. B. Wen, D. Boroyevich, R. Burgos, P. Mattavelli and Z. Shen, "Small-Signal Stability Analysis of Three-Phase AC Systems in the Presence of Constant Power Loads Based on Measured d-q Frame Impedances," in IEEE Transactions on Power Electronics, vol. 30, no. 10, pp. 5952-5963, Oct. 2015.

[12]. L. Harnefors, M. Bongiorno and S. Lundberg, "Input-Admittance Calculation and Shaping for Controlled Voltage-Source Converters," in *IEEE Transactions on Industrial Electronics*, vol. 54, no. 6, pp. 3323-3334, Dec. 2007.

[13]. M. Cespedes and J. Sun, "Impedance Modeling and Analysis of Grid-Connected Voltage-Source Converters," in IEEE Transactions on Power Electronics, vol. 29, no. 3, pp. 1254-1261, March 2014.

[14]. M. K. Bakhshizadeh, X. Wang, F. Blaabjerg, J. Hjerrild, L. Kocewiak, C. L. Bak, and B. Hesselbæk, "Couplings in Phase Domain Impedance Modeling of Grid-Connected Converters," IEEE Trans. Power Electron, vol. 31, no. 10, pp. 6792–6796, 2016.

[15]. X. Wang, L. Harnefors and F. Blaabjerg, "Unified Impedance Model of Grid-Connected Voltage-Source Converters," in *IEEE Transactions on Power Electronics*, vol. 33, no. 2, pp. 1775-1787, Feb. 2018.

[16]. S. Shah and L. Parsa, "Impedance Modeling of Three-Phase Voltage Source Converters in DQ, Sequence, and Phasor Domains," in IEEE Transactions on Energy Conversion, vol. 32, no. 3, pp. 1139-1150, Sept. 2017.

[17]. A. Rygg, M. Molinas, C. Zhang and X. Cai, "A Modified Sequence-Domain Impedance Definition and Its Equivalence to the dq-Domain Impedance Definition for the Stability Analysis of AC Power Electronic Systems," in IEEE Journal of Emerging and Selected Topics in Power Electronics, vol. 4, no. 4, pp. 1383-1396, Dec. 2016.

[18]. C. Zhang, X. Cai, A. Rygg and M. Molinas, "Sequence Domain SISO Equivalent Models of a Grid-Tied Voltage Source Converter System for Small-Signal Stability Analysis," in IEEE Transactions on Energy Conversion, vol. 33, no. 2, pp. 741-749, June 2018.

[19]. R. D. Middlebrook, "Input filter considerations in design and application of switching regulators," in Proc. IEEE Ind. Appl. Soc. Annu. Meeting, 1976, pp. 91–107

[20]. J. Sun. "Impedance-Based Stability Criterion for Grid-Connected Inverters," IEEE Trans. Power Electron, vol.26, no. 11, pp. 3075–3078, 2011.

[21]. C. Desoer and Yung-Terng Wang, "On the generalized nyquist stability criterion," in IEEE Transactions on Automatic Control, vol. 25, no. 2, pp. 187-196, April 1980

[22]. H. Liu and X. Xie, "Impedance Network Modeling and Quantitative Stability Analysis of Sub-/Super-Synchronous Oscillations for Large-Scale Wind Power Systems," in *IEEE Access*, vol. 6, pp. 34431-34438, 2018.

[23]. H. Liu, X. Xie and W. Liu, "An Oscillatory Stability Criterion Based on the Unified dq-Frame Impedance Network Model for Power Systems With High-Penetration Renewables," in IEEE Transactions on Power Systems, vol. 33, no. 3, pp. 3472-3485, May 2018

[24]. E. Ebrahimzadeh, F. Blaabjerg, X. Wang and C. L. Bak, "Harmonic Stability and Resonance Analysis in Large PMSG-Based Wind Power Plants," in IEEE Transactions on Sustainable Energy, vol. 9, no. 1, pp. 12-23, Jan. 2018.

[25]. C. Zhang, X. Cai, Z. Li, A. Rygg and M. Molinas, "Properties and physical interpretation of the dynamic interactions between voltage source converters and grid: electrical oscillation and its stability control," in IET Power Electronics, vol. 10, no. 8, pp. 894-902, 30 6 2017.

[26]. S. Ma, H. Geng, L. Liu, G. Yang and B. C. Pal, "Grid-Synchronization Stability Improvement of Large Scale Wind Farm During Severe Grid Fault," in *IEEE Transactions on Power Systems*, vol. 33, no. 1, pp. 216-226, Jan. 2018.

[27]. L. Harnefors, "Modeling of Three-Phase Dynamic Systems Using Complex Transfer Functions and Transfer Matrices," IEEE Trans. Ind. Electron, vol. 54, no. 4, pp. 2239–2248, 2007.

[28]. Z.W Yao, P.G.Therond, and B.Davat, "Frequency Characteristic of AC Power System", IFAC 12th Triennial World Congress, Sydney, Australia, 1993, pp. 737-740.

[29]. G. C. Paap, "Symmetrical components in the time domain and their application to power network calculations," in *IEEE Transactions on Power Systems*, vol. 15, no. 2, pp. 522-528, May 2000.

[30]. C. Zhang, X. Cai, M. Molinas and A. Rygg, "On the Impedance Modeling

This article has been accepted for publication in a future issue of this journal, but has not been fully edited. Content may change prior to final publication. Citation information: DOI 10.1109/JESTPE.2019.2914560, IEEE Journal of Emerging and Selected Topics in Power Electronics

> REPLACE THIS LINE WITH YOUR PAPER IDENTIFICATION NUMBER (DOUBLE-CLICK HERE TO EDIT) <   14

and Equivalence of AC/DC Side Stability Analysis of a Grid-tied Type-IV Wind Turbine System," in IEEE Transactions on Energy Conversion. doi: 10.1109/TEC.2018.2866639 (online).

[31]. B. Wen, D. Boroyevich, R. Burgos, P. Mattavelli and Z. Shen, "Inverse Nyquist Stability Criterion for Grid-Tied Inverters," in *IEEE Transactions on Power Electronics*, vol. 32, no. 2, pp. 1548-1556, Feb. 2017.

[32]. F. Liu, J. Liu, H. Zhang and D. Xue, "Stability Issues of Z + Z Type Cascade System in Hybrid Energy Storage System (HESS)," in IEEE Transactions on Power Electronics, vol. 29, no. 11, pp. 5846-5859, Nov. 2014.

[33]. X. Wang, F. Blaabjerg and P. C. Loh, "An impedance-based stability analysis method for paralleled voltage source converters," 2014 International Power Electronics Conference (ECCE), Hiroshima, 2014, pp. 1529-1535.

[34]. Y. Liao and X. Wang, "General Rules of Using Bode Plots for Impedance-Based Stability Analysis," 2018 IEEE 19th Workshop on Control and Modeling for Power Electronics (COMPEL), Padua, 2018, pp. 1-6.

Chen Zhang received the B.Eng. degree from the China University of Mining and Technology, China, and the Ph.D. from Shanghai Jiao Tong University, China, in 2011 and 2018 respectively. He was a Ph.D. Visiting Scholar with the Department of Engineering Cybernetics, Norwegian University of Science and Technology (NTNU), Norway, in 2015. Currently, he is a Postdoctoral Research Fellow at NTNU. His research interest is modeling and stability analysis of VSCs-based energy conversion systems, where the aim is to reveal the fundamental dynamics and stability mechanisms behind the grid-tied VSCs.

Marta Molinas (M'94) received the Diploma degree in electromechanical engineering from the National University of Asuncion, Asuncion, Paraguay, in 1992; the Master of Engineering degree from Ryukyu University, Japan, in 1997; and the Doctor of Engineering degree from the Tokyo Institute of Technology, Tokyo, Japan, in 2000. She was a Guest Researcher with the University of Padova, Padova, Italy, during 1998. From 2004 to 2007, she was a Postdoctoral Researcher with the Norwegian University of Science and Technology (NTNU) and from 2008-2014 she has been professor at the Department of Electric Power Engineering at the same university. She is currently Professor at the Department of Engineering Cybernetics, NTNU. Her research interests include stability of power electronics systems, harmonics, instantaneous frequency, and non-stationary signals from the human and the machine. She is Associate Editor for the IEEE Journal JESTPE, IEEE PELS Transactions and Editor of the IEEE Transactions on Energy Conversion. Dr. Molinas has been an AdCom Member of the IEEE Power Electronics Society from 2009 to 2011.

Atle Rygg received the MSc degree in Electrical Engineering from the Norwegian University of Science and Technology (NTNU) in 2011. From 2011 to 2015 he was a research scientist at SINTEF Energy Research in the field of power electronics. He received his Ph.D. at department of engineering cybernetics at NTNU, 2018. His topic or research is impedance-based stability analysis of power electronic systems, where the aim is to contribute to the fundamental understanding in this family of methods.

Xu Cai received the B.Eng. degree from Southeast University, Nanjing, China, in 1983, and the M.Sc. and Ph.D. degrees from the China University of Mining and Technology, Xuzhou, China, in 1988 and 2000, respectively. He was with the Department of Electrical Engineering, China University of Mining and Technology, as an Associate Professor from 1989 to 2001. He was the Vice Director of the State Energy Smart Grid R&D Center, Shanghai, China, from 2010 to 2013. He has been with Shanghai Jiao Tong University, Shanghai, as a Professor since 2002, where he has also been the Director of the Wind Power Research Center since 2008. His current research interests include power electronics and renewable energy exploitation and utilization, including wind power converters, wind turbine control system, large power battery storage systems, clustering of wind farms and its control system, and grid integration.